DNA Binding in the Central Channel of Bacteriophage T7 Helicase-Primase Is a Multistep Process. Nucleotide Hydrolysis Is Not Required†

Kristen Moore Picha,‡ Peter Ahnert,§ and Smita S. Patel*,‡

Departments of Biochemistry, Robert Wood Johnson Medical School, Piscataway, New Jersey 08854-5635, and The Ohio State University, Columbus, Ohio 43210

Received December 13, 1999; Revised Manuscript Received February 15, 2000

ABSTRACT: Many helicases assemble into ring-shaped hexamers and bind DNA in their central channel. This raises the question as to how the DNA gets into the central channel to form a topologically linked complex. We have used the presteady-state stopped-flow kinetic method and protein fluorescence changes to investigate the mechanism of single-stranded DNA (ssDNA) binding to the bacteriophage T7 helicase-primase, gp4A′. We have found that the kinetics of 30-mer ssDNA binding to a preformed gp4A′ hexamer in the presence of both Mg−dTMP-PCP and Mg−dTTP are similar, indicating that Mg−dTTP binding is sufficient and hydrolysis is not necessary for efficient DNA binding. Multiple transient changes in gp4A′ fluorescence revealed a four-step mechanism for DNA binding with Mg−dTTP. These transient changes were analyzed by global fitting and kinetic simulation to determine the intrinsic rate constants of this four-step mechanism. The initial steps, including the bimolecular encounter of the DNA with the helicase and a subsequent conformational change, were fast. We propose that these initial steps of DNA binding occur at a readily accessible site, which is likely to be on the outside of the hexamer ring. The binding of the 30-mer ssDNA at this loading site is followed by slower conformational changes that allow the DNA to transit into the central channel of gp4A′ via a ring-opening or threading pathway.

Helicases are ubiquitous enzymes that play an essential role in all processes of nucleic acid metabolism (*1, 2*). DNA helicases catalyze the unwinding of double-stranded DNA (dsDNA[1]) by unidirectional translocation on DNA and by destabilization of the intermolecular forces that maintain the duplex DNA structure. Helicases are motor proteins that couple the energy from NTPase turnovers to movement and unwinding of the dsDNA. A large number of helicases have been identified from various organisms at the present time, and the mechanisms of energy transduction and nucleic acid unwinding are being intensely studied in many different helicases.

Over the past decade a number of helicases, most of which are involved in DNA replication, have been shown to self-assemble into ring-shaped hexamers that have a central channel (*1, 2*). These helicases form hexamers in the absence of DNA, and most require only the presence of Mg^{2+} and/or NTP to form stable hexameric rings (*3*−*19*). The *Escherichia coli* helicases DnaB, RuvB, Rho, and bacteriophage T7 gp4 and T4 gp41 DNA helicases, SV40 large T-antigen, and bovine papilloma virus E1 helicases have been visualized by electron microscopy (*5, 9*−*11, 13, 14, 16, 20*−*24*). Many of these hexameric helicases, including bacteriophage T7 gp4A′, which is the subject of this study, have been proposed to bind DNA in the central channel (*13, 16, 21, 23, 25*−*27*). Because many of these proteins can form hexameric rings in the absence of DNA, mechanisms must exist for loading the DNA into the central channel of these rings. The studies presented here with T7 gp4A′ were carried out to elucidate such a loading mechanism. Similar to *E. coli* DnaB and T4 gp41, the T7 gp4 protein has been proposed to pass only one strand of the dsDNA through the central channel during DNA unwinding (*21, 23, 25, 26, 28*−*30*). The gp4A′ binds the 5′-DNA strand through the central channel and excludes the 3′-DNA strand (*31*). Although the exact mechanism of duplex melting is unknown, it has been proposed that translocation of the helicase on the DNA strand that passes through the central channel plays an important role in DNA unwinding.

In the present studies, we have used stopped-flow fluorescence experiments to gain insight into the kinetic mechanism of 30-mer ssDNA binding to a preformed hexamer of gp4A′. These studies were carried out with the goal of understanding the events that occur during the initiation of DNA unwinding and to dissect the steps that lead to binding of the ssDNA in the central channel. Analysis of the kinetic data revealed a four-step mechanism for DNA binding in the presence of Mg−dTTP, and global fitting provided the intrinsic rate constants of all steps. These studies revealed that the initial encounter of the DNA with the protein was very fast, and we propose that it occurred at a readily accessible site on the outside of the ring. The bimolecular encounter was followed by a fast conformational change, and the subsequent steps, proposed to represent migration

† This work was supported by National Institutes of Health Grant GM55310.

* Corresponding author. Telephone: 732-235-3372. Fax: 732-235-4783. E-mail: Patelss@umdnj.edu.

‡ Robert Wood Johnson Medical School.

§ The Ohio State University.

[1] Abbreviations: dsDNA, double-stranded DNA; ssDNA, single-stranded DNA; dTMP-PCP, deoxythymidine (β, γ, methylene) triphosphate.

10.1021/bi992857i CCC: $19.00
Published on Web 05/03/2000

of the DNA into the central channel, were much slower. Thus, even though the initial encounter with the DNA is fast, our studies predict that the formation of a productive helicase−DNA complex during initiation of DNA unwinding would be a slow process. Studies are underway to test this hypothesis.

EXPERIMENTAL PROCEDURES

Proteins and Enzymes. The gp4A′ was overexpressed, purified, and stored as described previously (*32*, *33*). The concentration of gp4A′ was determined both by absorbance measurements at 280 nm in 8 M urea (extinction coefficient: 76 100 M^{-1} cm^{-1}) and by the Bradford assay using BSA as a standard. Both methods of determining the concentration of gp4A′ gave similar results.

Nucleotides and Buffers. dTTP was purchased from Sigma, and dTMP-PCP was purchased from USB. Buffer H contains 50 mM NaCl, 20 mM TrisCl, pH 7.5 (tris(hydroxymethyl)-aminomethane chloride), and 10% glycerol.

Synthetic Oligodeoxynucleotides. A 30-mer ssDNA with the sequence 5′-ACA GTA CTC TAG TTA CTG ATC TGA GAT CAG-3′ was purchased from Integrated DNA Technologies and purified on a 15% polyacrylamide/3.2 M urea gel in TBE buffer. The 30-mer ssDNA band was excised, and the DNA was extracted by electroelution using an Elutrap apparatus from Schleicher & Schuell. The DNA was ethanol precipitated, and the concentration of the dissolved DNA was determined from the absorbance at 260 nm (in TE buffer containing 8 M urea) using a calculated extinction coefficient of 326 760 M^{-1} cm^{-1}.

Fluorescence Equilibrium Protein−DNA Binding. For equilibrium DNA binding fluorescence measurements, a solution containing 850 nM gp4A′ in buffer H with 2 mM Mg−dTMP-PCP and 9 mM $MgCl_2$ was excited at 295 nm, and the emission spectrum was recorded from 300 to 500 nm in a Fluoromax-2 fluorometer (Instruments SA, Inc.). The emission spectrum was collected again after 30-mer ssDNA (2 μM) was added to an identical sample. Both spectra were corrected for background fluorescence by subtracting the fluorescence spectrum of buffer H containing Mg−dTMP-PCP (2 mM) and $MgCl_2$ (9 mM). The fluorescence spectrum of protein in the presence of 30-mer ssDNA was also corrected for the inner filter effect due to DNA absorption at 295 nm using the following equation:

$$F_{c,i} = F_{o,i}(10^{0.5(A_x + A_{m,i})}) \quad (1)$$

$F_{c,i}$ is the corrected fluorescence intensity at a particular wavelength, i, $F_{o,i}$ is the observed fluorescence intensity, A_x is the absorbance of the DNA at 295 nm, and $A_{m,i}$ is the absorbance of the DNA at the emission wavelengths.

Stopped-Flow Fluorescence Experiments. The helicase−DNA binding kinetics were measured under pseudo-first-order conditions in a stopped-flow instrument manufactured by KinTek Corp., State College, PA. The dead time of the instrument was 2 ms, and the flow rate, 6 mL s^{-1}. A solution (40 μL) of gp4A′ (850 nM monomer), Mg−dTTP or Mg−dTMP-PCP (2 mM), and $MgCl_2$ (7 mM) in buffer H was rapidly mixed with a solution (40 μL) of 30-mer ssDNA (200 nM−10 μM), Mg−dTTP or Mg−dTMP-PCP (2 mM), and $MgCl_2$ (7 mM) in buffer H in the stopped flow instrument at 18 °C. The given concentrations are the final concentrations in the reaction. The fluorescence changes in gp4A′ were monitored using an excitation wavelength of 295 nm and monitoring the emission above 348 nm using a cutoff high pass filter (model no. 51260) from Oriel Corp. The upper limit of sensitivity of the photomultiplier tube was about 650 nm. A schematic of the experiment is outlined in Figure 2A. For each experiment, at least four fluorescence traces were averaged.

Several control experiments were carried out: (1) A solution containing the helicase, nucleotide, and $MgCl_2$ in buffer H was mixed with nucleotide and $MgCl_2$ in buffer H (without DNA). (2) A solution of helicase and $MgCl_2$ in buffer H (without nucleotide) was mixed with DNA and $MgCl_2$ in buffer H (without nucleotide). (3) Nucleotide and $MgCl_2$ in buffer H (without helicase) were mixed with DNA, nucleotide, and $MgCl_2$ in buffer H. No fluorescence changes were observed in these controls.

Determination of the Helicase−DNA Binding Mechanism. For the determination of the DNA binding mechanism, stopped-flow fluorescence experiments were carried out at increasing 30-mer ssDNA concentrations (see above). The averaged traces at each DNA concentration were fit to the sum of three exponentials to determine the rates of each phase (eq 2):

$$F = a_1 e^{-k_1 t} + a_2(1 - e^{-k_2 t}) + a_3(1 - e^{-k_3 t}) + C \quad (2)$$

F is the fluorescence as a function of time, a_1, a_2, and a_3 are the amplitudes, and k_1, k_2, and k_3 are the observed rate constants of the first, second, and third phases of the observed fluorescence changes, respectively. C is a constant. Due to the presence of a very fast and two relatively slow phases, data were collected in different time windows. At each concentration of DNA, two types of experiments were carried out. For accurate determination of the rate of the first phase, data were collected from 0 to 6 half-lives of the first phase in one window and up to 5 s in the second window. To determine more accurately the rates of the second and third phases, data were collected from 0 to 6 half-lives of the second phase, up to 6 half-lives of the third phase in the second window. In the presence of Mg−dTTP, both types of experiments were conducted for the entire range of DNA concentrations (0.2−8 μM). In the presence of Mg−dTMP-PCP, the first phase was accurately measured from 0.2 to 10 μM and the rest of the phases were measured from 0.2 to 2 μM concentration of DNA. The first and the second phases with Mg−dTTP were fit to the hyperbolic equation (eq 3).

$$k_{obs} = \frac{V_{max}[DNA]}{K_{1/2} + [DNA]} \quad (3)$$

V_{max} is the maximum observed rate, $K_{1/2}$ is the concentration of DNA at which the observed rate is half of the maximum observed rate, and k_{obs} is the observed rate.

Global Fitting of the Proposed Binding Mechanism to the Stopped-Flow Fluorescence Data. The intrinsic rate constants (Scheme 1) were determined by globally fitting the stopped-flow kinetic data collected at increasing concentrations of 30-mer ssDNA. The global nonlinear least-squares fitting

was carried out using the software "Scientist" (MicroMath Research, LC). Differential equations were written for each species in the mechanism shown in Scheme 1. For the global fitting, a separate set of differential equations, distinguished by different suffixes, was written for each DNA concentration. The stopped-flow fluorescence traces were directly fit by assigning the observed total fluorescence (FA) as the sum of the background fluorescence (FB), which is that part of the protein and buffer fluorescence that does not change due to ssDNA binding, and the contribution of each protein species to the total fluorescence at any reaction time *t*, specified by F through FD4:

$$\mathrm{FA} = F + \mathrm{FD1} + \mathrm{FD2} + \mathrm{FD3} + \mathrm{FD4} + \mathrm{FB}$$

where $F = EV$, FD1 = ED1·VD1, FD2 = ED2·VD2, FD3 = ED3·VD3, and FD4 = ED4·VD4.

V through VD4 are the values for the specific fluorescence of each helicase species. These specific fluorescence values describe only that part of the protein fluorescence that changes due to DNA binding. Differences in the inner filter effect for each species were accommodated by using different values for the specific fluorescence of a given species at different DNA concentrations. *E* through ED4 are the amounts of each protein species at any given time *t*. Initial values for the intrinsic rate constants k_1 through k_{-4} were estimated from the analysis of the plots of the observed rate constants versus the DNA concentration (Scheme 1). Initial values for the specific fluorescence of each species were set to 1, arbitrarily. First, the set of parameters for the intrinsic rate constants was kept constant and the specific fluorescence values were floated. Subsequently, one or the other set of parameters was kept constant and global fitting was used to optimize the floating set. The fitting process was governed by a modified Marquard−Levenberg algorithm, and the differential equations were numerically integrated using the stiff episode algorithm making use of the analytical Jacobian matrix. The quality of the fit was judged by visual inspection of overlays of the fitted curves and the data as well as inspection of the residuals.

RESULTS

The kinetics of ssDNA binding to a preformed hexamer of the T7 gp4A′ were investigated with the ultimate goal of understanding the mechanism of initiation of DNA unwinding. We know from previous studies that gp4A′ assembles into a stable hexamer in the presence of Mg−dTTP or Mg−dTMP-PCP, and the hexamer thus assembled is capable of binding a 30-mer ssDNA (*3*, *4*, *34*). Here we wished to elucidate the kinetic mechanism of 30-mer ssDNA binding to the gp4A′ hexamer. Often, binding of a ligand results in intrinsic protein fluorescence changes due to induced conformational changes in the protein. In such a case, the fluorescence changes can be used as reporters to determine the kinetics of ligand binding in real time using the stopped-flow kinetic method.

Protein Fluorescence Changes Due to DNA Binding. The fluorescence spectra of gp4A′ in the absence and presence of ssDNA were compared to explore possible fluorescence changes in T7 gp4A′ upon DNA binding. As shown in the individual spectra and the difference spectrum (Figure 1A),

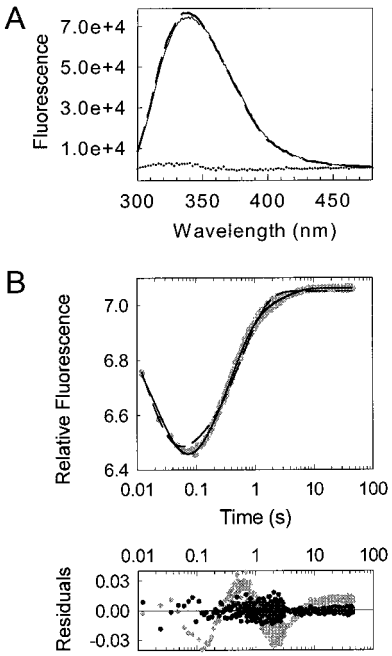

FIGURE 1: Change in the intrinsic protein fluorescence of gp4A′ upon 30-mer ssDNA binding. (A) The fluorescence spectra (excitation at 295 nm) of gp4A′, corrected for the inner filter effect, in the absence of DNA (thin, continuous line) and in the presence of DNA (thick, broken line) are shown. The difference spectrum is shown by the dotted line. (B) The transient changes in gp4A′ fluorescence upon 30-mer ssDNA binding are shown. These time-dependent changes were measured in a stopped-flow instrument at 18 °C by mixing gp4A′ (0.142 μM hexamer), Mg−dTTP (2 mM), and $MgCl_2$ (9 mM) from one syringe with 30-mer ssDNA (2 μM), Mg−dTTP (2 mM), and $MgCl_2$ (9 mM) from a second syringe. The above are final concentrations after mixing. The mixed solution was excited at 295 nm, and the protein fluorescence was monitored at >348 nm, from a few milliseconds to several seconds after mixing with the DNA. The fluorescence data are shown as gray circles. The data were fit to two and three exponentials (broken and continuous lines, respectively). The residuals for the fit to two and three exponentials (gray diamonds and black circles, respectively) illustrate the necessity for using a three-exponential fit.

the gp4A′ fluorescence increased very little upon DNA binding. In contrast, when the fluorescence of gp4A′ was measured by the stopped-flow method, relatively large changes in protein fluorescence were observed during the first few seconds after mixing gp4A′ with the DNA (Figure 1B). The fluorescence of gp4A′ decreased rapidly and then increased back to almost the initial value. The net change in protein fluorescence was small, consistent with the small change observed in the equilibrium fluorescence experiment. The decrease and increase in fluorescence with time fit best to a sum of three exponentials rather than two exponentials as shown by the plot of the residuals in Figure 1B.

The time-dependent stopped-flow experiments were also carried out using various fluorescent DNA molecules. The changes in the fluorescence of these DNAs upon formation of a protein−DNA complex were monitored (data not shown). No fluorescence changes were observed in the stopped-flow instrument when hexameric gp4A′ was mixed with etheno-dA−DNA (internally labeled) or amino-purine−DNA (internally labeled). When hexameric gp4A′ was mixed with fluorescein−DNA (fluorescein at the end), fluorescence changes were observed. However, they were sensitive to the position of the fluorescein moiety (5′-end or 3′-end) and did not show all of the phases obtained by monitoring the

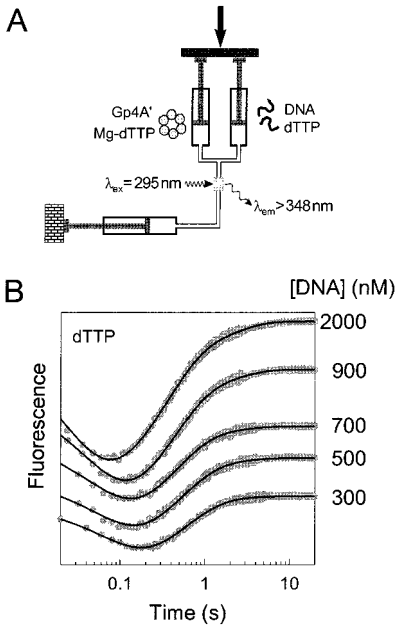

FIGURE 2: Stopped-flow kinetics of DNA binding in the presence of Mg−dTTP at increasing 30-mer ssDNA concentrations. (A) The cartoon shows the design of the stopped-flow experiment. A motor drive rapidly pushes the contents of two syringes through a flow cell into a third syringe, which stops the flow and mixes both solutions in the flow cell. The reaction occurring in the flow cell can be observed by fluorescence measurements (excitation wavelength, 295 nm; emission, >348 nm). (B) The gp4A′ (0.142 μM hexamer) was preincubated with Mg−dTTP (2 mM) and $MgCl_2$ (9 mM) in one syringe, and a mixture of 30-mer ssDNA, Mg−dTTP (2 mM), and $MgCl_2$ (9 mM) was added from the other syringe. The above are final concentrations after mixing. The resulting time courses of transient fluorescence changes with increasing 30-mer ssDNA concentrations (0.3−2 μM) are shown (gray circles). The time axis is in the log scale, and the solid black lines are the predicted kinetic curves according to the DNA binding mechanism shown in Scheme 1.

enzyme fluorescence. Therefore, monitoring protein fluorescence was the best method for measuring DNA binding to hexameric gp4A′.

The time-dependent fluorescence changes were observed only with ssDNA and only in the presence of Mg−dTTP or Mg−dTMP-PCP. These are conditions under which gp4A′ is known to be a hexamer (*3*) and interact with ssDNA (*4, 34*). No time-dependent fluorescence changes were observed when ssDNA in one syringe was mixed with gp4A′ and Mg−dTDP or with magnesium ions alone (data not shown). These results are consistent with previous observations that the gp4A′ hexamer interacts weakly with a 30-mer ssDNA in the presence of Mg−dTDP (*4, 34*). No fluorescence changes were observed when gp4A′ was mixed in the stopped-flow with a dsDNA hairpin in the presence of either Mg−dTMP-PCP or Mg−dTTP (data not shown). The hairpin structure was used to ensure that there was no free ssDNA in the reaction. These results are consistent with the previously reported data showing that the dsDNA interacts weakly with gp4A′ (*34*).

Four-Step Mechanism for DNA Binding in the Presence of Mg−dTTP. To determine the kinetic mechanism of 30-mer ssDNA binding to the gp4A′ hexamer, stopped-flow experiments were carried out at increasing 30-mer concentrations. These experiments determined the number of intermediate species in the DNA binding pathway and the rates of their formation and disappearance. The gp4A′ (142 nM hexamer) was preincubated with Mg−dTTP (2 mM) in syringe A of the stopped-flow instrument. The resulting hexamer was then rapidly mixed with a solution of 30-mer ssDNA from syringe B (Figure 2A). Upon mixing of the samples, several transient changes in the intrinsic protein fluorescence of gp4A′ were observed, and these were recorded in real time as shown in Figure 2B. The protein fluorescence decreased rapidly after mixing with the DNA and then more slowly increased to the original level of fluorescence. Representative stopped-flow traces at increasing 30-mer ssDNA concentrations (0.3−2.0 μM) are shown in Figure 2B. The kinetics traces from 0.3 to 8.0 μM were fit to the sum of three exponentials (eq 2), and the exponential rate constants were plotted versus the 30-mer ssDNA concentration to obtain the dependencies shown in Figure 3A−C.

The mechanism of DNA binding and the intrinsic rate constants govern the observed kinetics. Therefore, a quantitative analysis of the observed DNA concentration dependencies can provide that mechanism. The presence of three phases indicated that at least three steps and two intermediate species were present in the pathway of DNA binding. The observed rate of the first phase increased linearly with DNA concentrations up to 1 μM, with a slope equal to 2.5×10^7 M^{-1} s^{-1} (Figure 3A). This indicates that the formation of the first protein−DNA species is limited by a bimolecular step at 2.5×10^7 M^{-1} s^{-1}. At DNA concentrations greater than 1 μM the first phase began to saturate, and the entire dependence fit to a hyperbola. The hyperbolic dependence of the first fluorescence phase implies that there are two steps in the initial DNA-binding process. The first step is the bimolecular encounter between the helicase and the DNA, and this is followed by a conformational change. The hyperbola saturated at about 106 s^{-1} (the V_{max} of the hyperbolic fit; Figure 3A), which is an estimate for the rate of the conformational change in the forward direction (Scheme 1). The second phase increased in a hyperbolic manner as the DNA concentration was increased and saturated at 2.6 s^{-1} (Figure 3B). The hyperbolic DNA dependence of the second phase provided evidence for a third step in the DNA-binding pathway. This third step is a distinct conformational change that occurs with a forward rate close to 2.6 s^{-1}. The third phase remained nearly constant with increasing DNA at about 0.5 s^{-1} (Figure 3C), indicating that there is a fourth step in the DNA-binding pathway with a forward rate of approximately 0.5 s^{-1}.

The above semiquantitative analysis of the DNA concentration dependencies showed that the DNA-binding mechanism with Mg−dTTP consists of at least four steps. This mechanism is outlined in Scheme 1, where E represents gp4A′ hexamer, D is the free ssDNA, ED1 is the product of the bimolecular encounter, and ED2, ED3, and ED4 are subsequent states of the helicase−DNA complex. A forward and a reverse rate constant characterize each step in this mechanism, denoted as k_i through k_{-i}. The semiquantitative analysis described above provided rough estimates for the intrinsic rate constants in the forward direction as listed in Scheme 1, but the reverse rate constants could not be determined accurately without solving the explicit equations describing the mechanism. The four-step mechanism presents a challenge in terms of determining the intrinsic rate

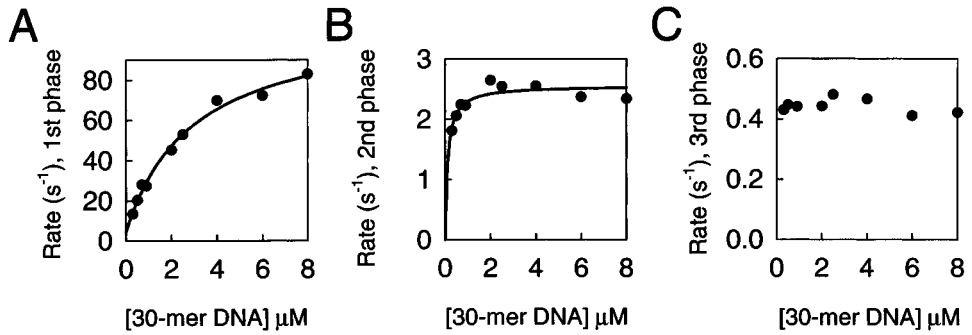

FIGURE 3: Rate constants as a function of the 30-mer ssDNA concentration dependence in the presence of Mg−dTTP. The kinetic traces at increasing concentrations of 30-mer ssDNA (0.2−8 μM) were fit to the sum of three exponentials (eq 2). The rate constants for each phase were plotted versus the 30-mer ssDNA concentration. (A) The rate of the first phase increased hyperbolically with increasing DNA. The fit of the data to a hyperbola (eq 3) provided a $K_{1/2}$ of 2.9 μM, a maximum rate of 106 s^{-1}, and a *y*-intercept of 4.5 s^{-1}. (B) The rate of the second phase increased hyperbolically with the DNA concentration and reached a maximum rate of 2.6 s^{-1} (*y*-intercept = 0). (C) The rate of the third phase remained constant at about 0.5 s^{-1}.

constants because an explicit solution for a reversible four-step DNA binding pathway with eight intrinsic rate constants cannot be determined. We therefore used the method of numerical integration and global fit of the kinetic data at various DNA concentrations to obtain the intrinsic rate constants, k_i-k_{-i}.

Global Fit To Obtain the Intrinsic Rate Constants. The four-step DNA-binding mechanism shown in Scheme 1 was expressed in terms of protein fluorescence changes occurring as a function of time. This procedure is described briefly below and in more detail in the Experimental Procedures. In the stopped-flow experiments, the observed fluorescence is the sum of the background fluorescence of the reaction mixture and the fluorescence of each helicase species present at a particular time. The background fluorescence, and part of the protein fluorescence, are constant through the time course of the experiment. However, changes in the observed fluorescence occur because part of the protein fluorescence is affected by ssDNA binding. Therefore, the observed fluorescence throughout a time course is determined by the accumulation of the different species, which can be described by differential equations. Instead of an explicit solution of these equations, numerical integration of the differential equations was used to fit the stopped-flow kinetic traces and determine the intrinsic rate constants.

The initial conditions were specified according to the reaction conditions (see Experimental Procedures). Initial values were estimated for the parameters (the intrinsic rate constants, the specific fluorescence values, and the background fluorescence). Estimates for the intrinsic rate constants were obtained from the analysis of the concentration dependence of the observed rate constants (Scheme 1). The initial values for the specific fluorescence of each species were set to unity, and those for the background fluorescence were estimated from the fluorescence traces. The experimental data for several DNA concentrations were fit simultaneously. The global fit uses a set of equations with several common parameters, which lowers the degrees of freedom for the overall fitting process. This global fitting approach also ensured that the derived model was consistent with the entire experimental data set. To facilitate the fitting process, an iterative approach was chosen, in which some of the parameters were fixed and others were optimized. Subsequently, the optimized parameters were fixed and the remaining ones were optimized, etc. Thus, a single set of

Scheme 1

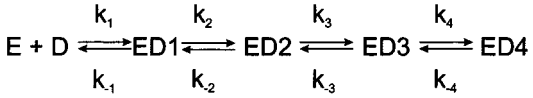

	dTTP		dTMP-PCP	
	3-exp. fit[1]	global fit[2]	3-exp. fit[1]	global fit[2]
k_1 ($M^{-1}s^{-1}$)	2.5 x 10^7	2.1 x 10^7	2 x 10^7	2.16 x 10^7
k_{-1} (s^{-1})	N/A	50.4	15.7	9.1
k_2 (s^{-1})	106	132.4	fast	fast
k_{-2} (s^{-1})	N/A	17.3	fast	fast
k_3 (s^{-1})	2.6	3.4	2.5	2.8
k_{-3} (s^{-1})	N/A	0.26	N/A	0.07
k_4 (s^{-1})	0.5	0.6	0.22	0.21
k_{-4} (s^{-1})	N/A	0	N/A	0

[1] These rate constants, obtained by analysis of the DNA concentration dependencies of the observed rate constants, were also used as estimates for the intrinsic rate constants during global fitting (Figure 3 for dTTP, Figure 5B for dTMP-PCP).
[2] Final values for the intrinsic rate constants were obtained by globally fitting data sets at increasing DNA concentrations.

rate constants and fluorescence factors was obtained that best described the experimental data.

The global fit provided the intrinsic rate constants of the four-step DNA binding mechanism in the presence of Mg−dTTP as shown in Scheme 1. These intrinsic rate constants were used to simulate the stopped-flow kinetics, shown as solid lines in Figure 2B. The final numbers provided a good agreement between the stopped-flow data and the simulated curves. The mechanism for DNA binding shows that the first two steps, comprising the initial DNA binding event to the hexamer, occur at relatively fast rates. The bimolecular encounter rate is close to diffusion-limited ($k_1 = 2.1 \times 10^7$ M^{-1} s^{-1}), and the dissociation of the resulting ED1 complex into its components is also fast with $k_{-1} = 50.4$ s^{-1}. Thus, the ED1 species has a weak K_d of 2.5 μM. ED1 converts to ED2 at a forward rate of $k_2 = 132$ s^{-1} and a reverse rate of $k_{-2} = 17$ s^{-1}. The ED2 intermediate subsequently converts to ED3 and ED4 at relatively slow rate constants ($k_3 = 3.5$ s^{-1}, $k_{-3} = 0.26$ s^{-1}, and $k_4 = 0.6$ s^{-1}). There was no detectable rate (k_{-4}) for the conversion of ED4 to ED3.

It should be pointed out that two ssDNA molecules can bind to a single gp4A′ hexamer at equilibrium (*34*). It may be argued that the observed fluorescence changes may be due to the binding of both of these two ssDNAs rather than only one, as proposed in Scheme 1. However, the K_d for the

second molecule of DNA which binds to gp4A′ was reported to be 5 μM (*34*). Since the stopped-flow experiments were carried out at DNA concentrations from 0.2 to 8 μM, binding of a second ssDNA should not occur at the lower DNA concentrations. Yet, all phases of the fluorescence changes were visible at all DNA concentrations (Figure 3). At higher concentrations of DNA, no additional phases were observed. We were able to globally fit the data to the linear mechanism in Scheme 1, and hence, it appears that the second DNA binding does not contribute in a significant way to the observed fluorescence changes.

Kinetic Mechanism of 30-mer ssDNA Binding in the Presence of Mg−dTMP-PCP. To determine if the DNA-binding process was facilitated by the Mg−dTTP hydrolysis reaction, the stopped-flow studies were carried out as described above with dTMP-PCP, the nonhydrolyzable analogue of dTTP. Previous studies have shown that the gp4A′ hexamer forms a very stable complex with ssDNA in the presence of Mg−dTMP-PCP (K_d = 100 nM) (*34*). However, it was not known if the mechanism of DNA-binding would be different in the presence of the nonhydrolyzable analogue. It was possible that the DNA binding process could be more efficient in the presence of Mg−dTTP, because nucleotide binds at the subunit interface (*27*), and hydrolysis of Mg−dTTP may facilitate the ring-opening step and thus promote faster binding of the DNA to the protein.

To determine the DNA-binding mechanism in the presence of Mg−dTMP-PCP, the stopped-flow experiments were carried out at increasing 30-mer ssDNA concentrations with 2 mM Mg−dTMP-PCP. We verified that 2 mM Mg−dTMP-PCP was saturating, by conducting stopped-flow experiments from 2.5 μM to 2 mM Mg−dTMP-PCP, and no significant changes in the rates of 30-mer ssDNA binding were observed (data not shown). The kinetics of DNA binding with Mg−dTMP-PCP showed three phases of changing fluorescence (Figure 4A). A decrease in fluorescence was observed in the first phase, which was followed by two phases of increasing fluorescence. Figure 4B−D shows the DNA concentration dependence of the rate constants of the three phases. The observed rates of these phases were very close to those in the presence of Mg−dTTP. This indicated that the intermediate species in the presence of Mg−dTMP-PCP were the same as those in the presence of Mg−dTTP. The only difference in the DNA binding kinetics with Mg−dTMP-PCP versus Mg−dTTP was in the DNA concentration dependence of the first phase (Figure 4B). In contrast to the hyperbolic change observed in the presence of Mg−dTTP, the rate of the first phase increased in a linear manner in the presence of Mg−dTMP-PCP, in the range of DNA concentrations used. We did not attempt to see if the rates would saturate at higher concentrations of DNA because it required a large amount of material. The linear DNA dependence in the presence of Mg−dTMP-PCP indicates that the transition from ED1 to ED2 is faster with Mg−dTMP-PCP than with Mg−dTTP. Thus, in the range of DNA concentrations used, the ED1 species does not accumulate measurably and is not observed in the kinetics.

The intrinsic rate constants of the DNA binding mechanism with Mg−dTMP-PCP were determined using the method of numerical integration and global fitting. The final mechanism in Scheme 1 shows that the initial DNA binding

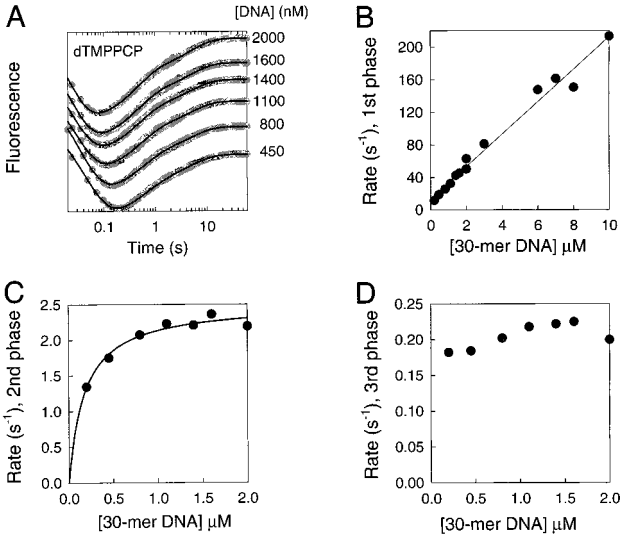

FIGURE 4: Stopped-flow kinetics of 30-mer ssDNA binding in the presence of Mg−dTMP-PCP. The experimental conditions were the same as in Figure 2A, except 2 mM Mg−dTMP-PCP was used instead of Mg−dTTP. (A) The time courses of fluorescence changes at increasing 30-mer ssDNA concentrations in the presence of Mg−dTMP-PCP are shown (gray circles). The time axis is in a log scale, and the solid black lines are the predicted kinetic curves according to the DNA-binding mechanism with Mg−dTMP-PCP shown in Scheme 1. The plots in (B)−(D) show the 30-mer ssDNA concentration dependence of the rate constants obtained from the fit of the kinetic traces in (A) to eq 2. The rate of the first phase increased linearly with increasing concentrations of DNA, the slope provided a k_{on} of 2×10^7 M^{-1} s^{-1}, and the *y*-intercept provided a k_{off} of 15.7 s^{-1}. The rate of the second phase increased hyperbolically with the concentration of DNA and reached a maximum rate of 2.5 s^{-1} (*y*-intercept = 0). The rate of the third phase remained constant at about 0.2 s^{-1}.

event, which results in ED1, is fast with $k_1 = 2.2 \times 10^7$ M^{-1} s^{-1} and $k_{-1} = 9$ s^{-1}. The conversion of ED1 to ED2 is a fast step; thus, the forward and reverse rate constants could not be assigned. An estimate for the lower limit of k_2 is 200 s^{-1}, since the rate of the first phase remains linear up to the highest measured DNA concentration. The last two steps occurred at almost the same rates as with Mg−dTTP, $k_3 = 2.8$ s^{-1}, $k_{-3} = 0.07$ s^{-1}, $k_4 = 0.2$ s^{-1}, and $k_{-4} = 0$. These results indicate that DNA binding occurs by the same mechanism (Scheme 1), even in the absence of Mg−dTTP hydrolysis. In the presence of Mg−dTMP-PCP, the rate constants for the second step are increased in comparison to Mg−dTTP. This is the opposite of what would be expected if Mg−dTTP hydrolysis facilitated DNA binding. In the presence of Mg−dTMP-PCP, the observed increase in the rate constants for the second step may be due to the different structure of the nucleotide. Therefore, Mg−dTTP hydrolysis does not appear to play a role in the DNA-binding process.

Kinetics of 30-mer ssDNA Binding as a Function of Protein Concentration. To investigate if gp4A′ hexamerization played a role in the observed DNA binding kinetics, the stopped-flow kinetic experiments were carried out at increasing protein concentrations. We wanted to investigate if the mechanism of DNA binding involved disassembly and assembly of gp4A′ subunits around the DNA. In the stopped-flow experiments, we therefore kept the DNA concentration (1 μM) in excess of the protein concentration (8−400 nM). Under these conditions, the observed rate will be largely dictated by the concentration of the ligand that is in excess

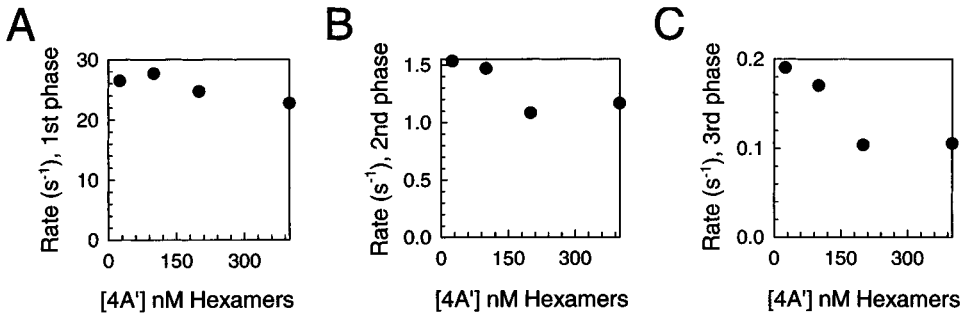

FIGURE 5: Kinetics of DNA binding as a function of gp4A′ concentration. The stopped-flow kinetics of 30-mer ssDNA binding were measured in the presence of 1 mM Mg−dTMP-PCP at constant 30-mer ssDNA (1 μM) and increasing gp4A′ (8−400 nM hexamer). The kinetic traces at various protein concentrations were fit to eq 2, and plots in (A)−(C) show the dependence of the observed rate constants of the three phases as a function of the gp4A′ hexamer concentration.

(which is DNA), and since the DNA concentration does not change, the observed rates are not expected to change significantly. Thus, if gp4A′ is a stable hexamer that does not disassemble and reassemble around the DNA, then the observed rates of DNA binding will change only slightly. However, if hexamer formation was occurring during DNA binding, a protein concentration dependence would be expected for the observed rates. Figure 5A−C shows the plot of each of the three rates at increasing gp4A′ hexamer concentration, in the presence of Mg−dTMP-PCP. The observed rates of the three phases change very little with protein concentration. The rate of the first fast phase remained constant at around 25 s^{-1}, and the subsequent phases, at 1.2 and 0.15 s^{-1}. These are the values expected at 1 μM 30-mer ssDNA concentration, as shown in Figure 4B−D. This protein concentration independence therefore indicates that gp4A′ is not disassembling and assembling around the DNA.

DISCUSSION

The results reported here establish the minimal mechanism of a 30-mer ssDNA binding to a preformed hexamer of T7 gp4A′. The kinetic pathway of 30-mer ssDNA binding was determined by following the transient changes in the intrinsic gp4A′ protein fluorescence upon DNA binding using the stopped-flow method. In these experiments, we have monitored the protein tryptophan fluorescence because the protein was excited at 295 nm. T7 gp4A′ has a total of 10 tryptophans, with 4 in the helicase domain and 6 in the N-terminal primase domain. The crystal structure of the helicase domain of T7 gp4A′ was recently solved (*27*). Although there are no tryptophans or tyrosines in the loop proposed to be involved in DNA binding, there are tryptophan residues close to the proposed subunit−subunit interface. The observed fluorescence changes could result from the disruption of a subunit interface, from global conformational changes in the protein upon DNA binding, or from both.

DNA Binding Kinetics with Mg−dTTP and Mg−dTMP-PCP. The kinetic pathway of 30-mer ssDNA binding was determined both in the presence of dTTP and its nonhydrolyzable analogue, dTMP-PCP. The elucidated kinetic pathways in the presence of either Mg−dTMP-PCP or Mg−dTTP were almost identical. With both, Mg−dTTP and Mg−dTMP-PCP, an initial close to diffusion-limited DNA binding step was observed. The second step in the DNA binding pathway was fast in the presence of Mg−dTTP and too fast to measure in the presence of Mg−dTMP-PCP. The rates of the two subsequent steps were slow and similar with both nucleotides. No DNA binding was observed in the presence of Mg−dTDP, although Mg−dTDP promotes hexamer formation of gp4A′ (*3*, *4*). This is consistent with previous results that showed very weak DNA binding with Mg−dTDP (*4*, *34*). The results from these studies indicate that Mg−dTTP or Mg−dTMP-PCP binding is necessary for DNA binding, but Mg−dTTP hydrolysis is not necessary for DNA binding.

Kinetic Mechanism of 30-mer ssDNA Binding. We have used numerical integration and global fitting to obtain the intrinsic rate constants of the four steps of 30-mer ssDNA binding (Scheme 1). The stopped-flow kinetic traces obtained at various DNA concentrations were globally fit to the four-step model. The constraints provided by the DNA concentration dependencies of the observed rate constants result in a more accurate determination of the intrinsic rate constants. The 30-mer ssDNA binding mechanism with Mg−dTTP consists of the following steps: The initial encounter of the DNA with the gp4A′ hexamer occurs at a close to diffusion-limited rate constant ($k_1 = 2.1 \times 10^7$ M^{-1} s^{-1}). The rate for the dissociation of this complex into its components is $k_{-1} = 50.4$ s^{-1}. The first protein−DNA complex, ED1, resulting from the bimolecular encounter, is transient and converts to ED2 at a forward rate of $k_2 = 132$ s^{-1} and a reverse rate of $k_{-2} = 17$ s^{-1}. This step was not observed and was considered to be fast with Mg−dTMP-PCP. The ED2 intermediate subsequently converts to ED3 and ED4 at rate constants that are relatively slow ($k_3 = 3.5$ s^{-1}, $k_{-3} = 0.26$ s^{-1}, and $k_4 = 0.6$ s^{-1}). Thus, k_3 and k_4 are the slowest forward rate constants in the pathway of DNA binding and may limit the overall process of DNA binding in the central channel of the gp4A′ hexamer. There was no detectable rate (k_{-4}) for the conversion of ED4 to ED3.

To better understand the relationship between the accumulated species and the observed fluorescence, the formation and decay of the various species and the observed fluorescence were simulated as a function of time for the DNA binding pathway with Mg−dTTP (Figure 6A). It is clear that the ED1 intermediate does not accumulate to a significant extent because it is rapidly converted to ED2. The intermediates ED2 and ED3 accumulate the most, and thus, the formation of ED4 occurs with a distinct lag. Only a part of the protein fluorescence changed upon ssDNA

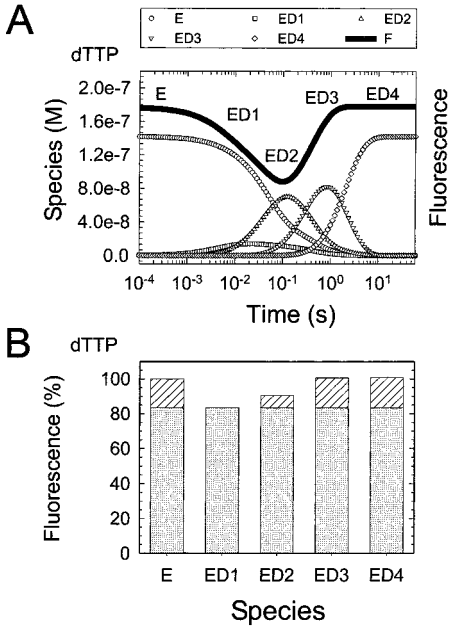

FIGURE 6: Kinetic simulation of 30-mer ssDNA binding to the gp4A′ hexamer in the presence of Mg−dTTP. (A) The formation and decay of various species in the DNA binding pathway with Mg−dTTP was simulated using the final intrinsic rate constants shown in Scheme 1. The concentrations of gp4A′ hexamer and DNA were 142 nM and 1 μM, respectively. Note that the time axis is shown in the logarithmic scale to enable better visualization of events occurring both at short and long times. The open circles show the decay of free protein (E). The squares, triangles (up), and triangles (down) show the formation and decay of the intermediates ED1, ED2, and ED3, respectively. The diamonds show the formation of the final, stably bound protein−DNA complex (ED4). The overall fluorescence change is represented by the solid black line and is scaled on an independent *y*-axis (fluorescence). (B) The bars show the total fluorescence of equal amounts of each pure species. The gray portions of the bars show the protein fluorescence (and the background) that does not change due to ssDNA binding. The hatched portions of the bars represent that part of the protein fluorescence that is affected by ssDNA binding. The total fluorescence of E was set to 100%.

binding, suggesting that the binding process does not affect all 10 tryptophans in gp4A′. The global fitting provided information about the proportion of the protein fluorescence that is affected by ssDNA binding (Figure 6B). ED1 has the lowest fluorescence of all species, but it does not contribute much to the observed fluorescence changes since it does not accumulate to a significant extent. Most of the decrease in fluorescence is due to the accumulation of ED2. The subsequent increase in fluorescence occurs because the fluorescence of ED3 and ED4 is similar to that of E.

Are the Proposed Intermediates Kinetically Competent? The proposed four-step model for 30-mer ssDNA binding of T7 gp4A′ is considerably more complex than a simple bimolecular DNA binding process. Two questions arise: First, are all of the proposed intermediates kinetically competent? Second, are there additional helicase−DNA intermediates that are needed to form a productive helicase−DNA complex but may not have been observable with the methods used here? The first question can be answered by determining whether each of the proposed intermediates is part of the kinetic pathway leading to a final species that exhibits all the functionally meaningful activities of the enzyme, such as dTTPase and helicase. The second question can be addressed by determining whether the proposed mechanism sufficiently describes the formation of such a productive helicase−DNA species. In case of T7 gp4A′, a productive species would be stably bound to ssDNA, able to unwind dsDNA, and hydrolyze Mg−dTTP at a stimulated level. The studies addressing these issues are in progress and will be reported elsewhere (*35*).

Fast DNA Binding Step Indicates the Presence of a Readily Accessible Site on the gp4A′ Hexamer. In the presence of either Mg−dTTP or Mg−dTMP-PCP, the bimolecular binding of DNA to the protein was observed as a very fast step, approaching the rate of diffusion (2×10^7 M^{-1} s^{-1}). The observation of a close to diffusion-limited binding of DNA to the hexamer in the first step suggested that a readily accessible site was available for DNA binding. If the DNA binding site was sterically occluded or hidden (either directly in the channel or in a transient site), many of the encounters between the DNA and the protein would be nonproductive and the bimolecular binding step would be much slower than the rate of diffusion. We argue that the DNA-binding site in the central channel of a preformed closed ring is not readily accessible and propose that the DNA first interacts with a readily accessible site on the outside of the ring.

Previous equilibrium DNA binding studies have shown that the gp4A′ hexamer binds two 30-mer ssDNA molecules, one with a tight K_d (100 nM) and a second with a 50-fold weaker K_d (*34*). The DNA-binding site in the central channel is most likely the tight one, and the weaker DNA binding site may be located on the outside of the ring. This weaker site on the outside of the ring would be readily accessible for fast DNA binding. There are six potential DNA binding sites, and this would make the initial binding process a very fast step. The only known DNA binding site that has been proposed to be located on the outside of the gp4A′ ring is the primase site (*36*). It is therefore possible that the primase site serves as a loading site and facilitates the binding of DNA in the central channel.

There are several kinetic pathways starting from a preformed hexamer by which DNA can bind in the central channel. A small oligo such as a 30-mer can thread into the central channel of a closed ring through one of its ends. Alternatively, the hexamer ring has to open in order for the DNA to access the site in the central channel, or the hexamer can disassemble and then reassemble around the DNA. We have eliminated the mechanism in which gp4A′ subunits assemble around the DNA, on the basis of two results: First, the DNA binding kinetics under the conditions of excess DNA were independent of the gp4A′ concentration, as shown in Figure 5. Second, we have shown previously, using an inactive mutant of gp4A′ that is capable of forming mixed hexamers and inactivating the wild-type 4A′ activity, that the subunits of a preformed hexamer do not exchange during the DNA binding process (*37*). Therefore, disassembly and assembly of subunits does not occur during the DNA binding process, and the threading and the ring-opening are the only possible mechanisms for a 30-mer ssDNA binding to a preformed ring. As discussed above, we have proposed that the initial interaction of the DNA occurs at an easily accessible site on the outside of the ring. Hence, the simplest threading and ring-opening mechanisms require additional steps in which a DNA first binds on the outside of the ring. The DNA that is already bound to the outside either threads into the closed ring or the ring opens and the DNA transits

into the central channel of the open ring. We can therefore propose that the ED1 species represents a helicase−DNA complex in which the DNA is bound on the outside, and the subsequent species represent different conformational states of the helicase−DNA complex that are necessary for the DNA to bind in the central channel.

ACKNOWLEDGMENT

We thank Dr. Susan Gilbert and Dr. Manju Hingorani for their comments and the members of the Patel lab for helpful discussions and Dr. Francesco Antonuccio for help with the mathematical background.

REFERENCES

1. Matson, S. W., and Kaiser-Rogers, K. A. (1990) *Ann. Rev. Biochem. 59*, 289−329.
2. Lohman, T. M., and Bjornson, K. P. (1996) *Ann. Rev. Biochem. 65*, 169−214.
3. Patel, S. S., and Hingorani, M. M. (1993) *J. Biol. Chem. 268*, 10668−10675.
4. Picha, K. M., and Patel, S. S. (1998) *J. Biol. Chem. 273*, 27315−27319.
5. Gogol, E. P., Seifried, S. E., and von Hippel, P. H. (1991) *J. Mol. Biol. 221*, 1127−1138.
6. Bujalowski, W., Klonowska, M. M., and Jezewska, M. J. (1994) *J. Biol. Chem. 269*, 31350−31358.
7. Reha-Krantz, L. J., and Hurwitz, J. (1978) *J. Biol. Chem. 253*, 4043−4050.
8. Arai, K., Yasuda, S., and Kornberg, A. (1981) *J. Biol. Chem. 256*, 5247−5252.
9. San Martin, M. C., Stamford, N. P., Dammerova, N., Dixon, N. E., and Carazo, J. M. (1995) *J. Struct. Biol. 114*, 167−176.
10. Yu, X., Jezewska, M. J., Bujalowski, W., and Egelman, E. H. (1996) *J. Mol. Biol. 259*, 7−14.
11. San Martin, C., Radermacher, M., Wolpensinger, B., Engel, A., Miles, C. S., Dixon, N. E., and Carazo, J. M. (1998) *Structure 6*, 501−509.
12. Mitchell, A. H., and West, S. C. (1994) *J. Mol. Biol. 243*, 208−215.
13. Stasiak, A., Tsaneva, I. R., West, S. C., Benson, C. J., Yu, X., and Egelman, E. H. (1994) *Proc. Natl. Acad. Sci. U.S.A. 91*, 7618−7622.
14. San Martin, M. C., Gruss, C., and Carazo, J. M. (1997) *J. Mol. Biol. 268*, 15−20.
15. Dean, F. B., Dodson, M., Echols, H., and Hurwitz, J. (1987) *Proc. Natl. Acad. Sci. U.S.A. 84*, 8981−8985.
16. Mastrangelo, I. A., Hough, P. V., Wall, J. S., Dodson, M., Dean, F. B., and Hurwitz, J. (1989) *Nature 338*, 658−662.
17. Parsons, R. E., Stenger, J. E., Ray, S., Welker, R., Anderson, M. E., and Tegtmeyer, P. (1991) *J. Virol. 65*, 2798−2806.
18. Dean, F. B., Borowiec, J. A., Eki, T., and Hurwitz, J. (1992) *J. Biol. Chem. 267*, 14129−14137.
19. Wessel, R., Schweizer, J., and Stahl, H. (1992) *J. Virol. 66*, 804−815.
20. Wessel, R., Ramsperger, U., Stahl, H., and Knippers, R. (1992) *Virology 189*, 293−303.
21. Egelman, E. H., Yu, X., Wild, R., Hingorani, M. M., and Patel, S. S. (1995) *Proc. Natl. Acad. Sci. U.S.A. 92*, 3869−3873.
22. Dong, F., Gogol, E. P., and von Hippel, P. H. (1995) *J. Biol. Chem. 270*, 7462−7473.
23. Yu, X., Hingorani, M. M., Patel, S. S., and Egelman, E. H. (1996) *Nat. Struct. Biol. 3*, 740−743.
24. Fouts, E. T., Yu, X., Egelman, E. H., and Botchan, M. R. (1999) *J. Biol. Chem. 274*, 4447−4458.
25. Morris, P. D., and Raney, K. D. (1999) *Biochemistry 38*, 5164−5171.
26. Bujalowski, W., and Jezewska, M. J. (1995) *Biochemistry 34*, 8513−8519.
27. Sawaya, M. R., Guo, S., Tabor, S., Richardson, C. C., and Ellenberger, T. (1999) *Cell 99*, 167−177.
28. Yong, Y., and Romano, L. J. (1996) *Chem. Res. Toxicol. 9*, 179−187.
29. Hacker, K. J., and Johnson, K. A. (1997) *Biochemistry 36*, 14080−14087.
30. Raney, K. D., Carver, T. E., and Benkovic, S. J. (1996) *J. Biol. Chem. 271*, 14074−14081.
31. Ahnert, P., and Patel, S. S. (1997) *J. Biol. Chem. 272*, 32267−32273.
32. Patel, S. S., Rosenberg, A. H., Studier, F. W., and Johnson, K. A. (1992) *J. Biol. Chem. 267*, 15013−15021.
33. Hingorani, M. M., and Patel, S. S. (1996) *Biochemistry 35*, 2218−2228.
34. Hingorani, M. M., and Patel, S. S. (1993) *Biochemistry 32*, 12478−12487.
35. Ahnert, P., Picha, K. M., Patel, S. S. (2000) *EMBO J.*, in press.
36. Kusakabe, T., Baradaran, K., Lee, J., and Richardson, C. C. (1998) *EMBO J. 17*, 1542−1552.
37. Patel, S. S., Hingorani, M. M., and Ng, W. M. (1994) *Biochemistry 33*, 7857−7868.

BI992857I